

Chapter 7

Very high precision bound state spectroscopy near a ^{85}Rb Feshbach resonance

7.1 Atom-molecule coherence as a novel Feshbach resonance probe

7.1.1 Introduction

The phenomenon of a Feshbach resonance in ultracold collisions of alkali atoms has received much theoretical and experimental interest in recent years and has sparked interest in the subject of resonant Bose-Einstein condensates (BEC). In addition to providing the subject matter for this thesis, Feshbach resonances were used to control elastic and inelastic collisions in ultracold gases [74, 75, 76, 77] and for tuning the self-interaction in BEC [12, 26, 2] by changing the magnitude of an external magnetic field.

The magnetic field controls the self-interaction in the BEC by affecting the s-wave scattering length, a . Close to resonance, the scattering length varies with B-field according to

$$a = a_{\text{bg}} \left(1 - \frac{\Delta}{B - B_{\text{peak}}} \right), \quad (7.1)$$

where B_{peak} is the resonance position and is defined to be the magnetic field where the magnitude of a becomes infinite, a_{bg} is the background scattering length, and $\Delta = B_{\text{zero}} - B_{\text{peak}}$ is the resonance width where B_{zero} is the B-field where the scattering length crosses zero. Measurements of Feshbach resonance positions and widths have

been used in a variety of alkali atoms to improve the determination of the interatomic potentials. These potentials have then been used to precisely calculate a multitude of important properties for trapped atomic gases [75, 78, 79, 13, 77, 69].

In ^{85}Rb , our recent production of an atom-molecule superposition state has allowed us to dramatically improve an existing determination of the Feshbach resonance position and width. The phenomenon of atom-molecule coherence was described in detail in Chapter 6. By inducing periodic oscillations in the number of condensate atoms, we obtain a direct, high precision measurement of the molecular bound state energy. Exploiting the resonance, we tune the molecular state very close to threshold — to our knowledge, this is the most weakly bound state ever observed.

This chapter discusses the experimental techniques for mapping out the B-field dependence of the molecular binding energy and how the data were fit to a theoretical model based on 2-body scattering theory. As a result of the fitting, there was a substantial improvement in the determination of the Feshbach resonance parameters. The strengths and limitations of the present method for studying the Feshbach resonance are emphasized. The final section of the chapter discusses our search for many-body effects, which manifest themselves in a mean-field shift to the observed oscillation frequency.

7.1.2 Sensitivity of binding energy to Feshbach resonance parameters

The atom-molecule coherent oscillation frequency, ν_0 , is directly related to the molecular state binding energy by $\epsilon_{\text{bind}} = \nu_0/h$. Since the magnitude of this binding energy depends strongly on the distance from the Feshbach resonance, one can use measurements of the binding energy and corresponding magnetic field to constrain the Feshbach resonance parameters, such as the position (B_{peak}), width (Δ), and background scattering length (a_{bg}). To understand the close relationship between ϵ_{bind} and the Feshbach resonance parameters, it is useful to consider the approximate expression

$$\epsilon_{\text{bind}} = -\hbar^2/(ma^2), \quad (7.2)$$

which is valid when the scattering length, a , is large and positive.¹ Substituting equation (7.1) for a versus B-field into equation (7.2) leads to an equation relating the oscillation frequency to the Feshbach resonance parameters:

$$\nu_0 = \frac{\hbar}{2\pi m a_{bg}^2} \frac{(B - B_{peak})^2}{(B - B_{zero})^2}. \quad (7.3)$$

For magnetic field changes near resonance ($B \geq B_{peak}$), the numerator of equation (7.3) varies much more rapidly than the denominator and the B-field dependence is nearly quadratic. To first approximation, a plot of binding energy versus B-field is simply a parabola centered at B_{peak} and with a curvature that depends on $1/a_{bg}^2$. Clearly, one can obtain information about the Feshbach resonance parameters from the magnetic field dependence of ϵ_{bind} , as indicated schematically in Figure 7.1.

One of the best uses we found for equation (7.3) was to determine the optimal data-gathering strategy for precisely determining a given Feshbach resonance parameter. For example, if we hold other parameters fixed, B_{peak} can be best determined by measurements of high oscillation frequencies, where the slope $\Delta\nu_0/\Delta B$ is large. Using simple error propagation and making reasonable assumptions for experimental uncertainties in a typical (B, ν_0) measurement, we estimated that we should be able to measure B_{peak} to a precision of 0.047 G and a_{bg} to a precision of $4.5 a_0$. Although these estimates turned out to be fairly conservative (see section 7.3.3), they motivated us to pursue the measurement because such precision would represent a dramatic improvement over that obtained in earlier experiments (0.4 G for B_{peak} and $21 a_0$ for a_{bg} [1]).

Although the present discussion of equation (7.3) provides motivation for precise measurements of the binding energy, the actual theoretical analysis used to model the data was considerably more complex. Servaas Kokkelmans collaborated with us to model the binding energy data. He utilized a highly accurate coupled-channels scattering model to fit the experimental data and extract the Feshbach resonance parameters,

¹ In fact, equation (7.2) only underestimates the actual binding energy by $\sim 30\%$ for $a \simeq 300 a_0$ ($B \simeq 161.5$ G).

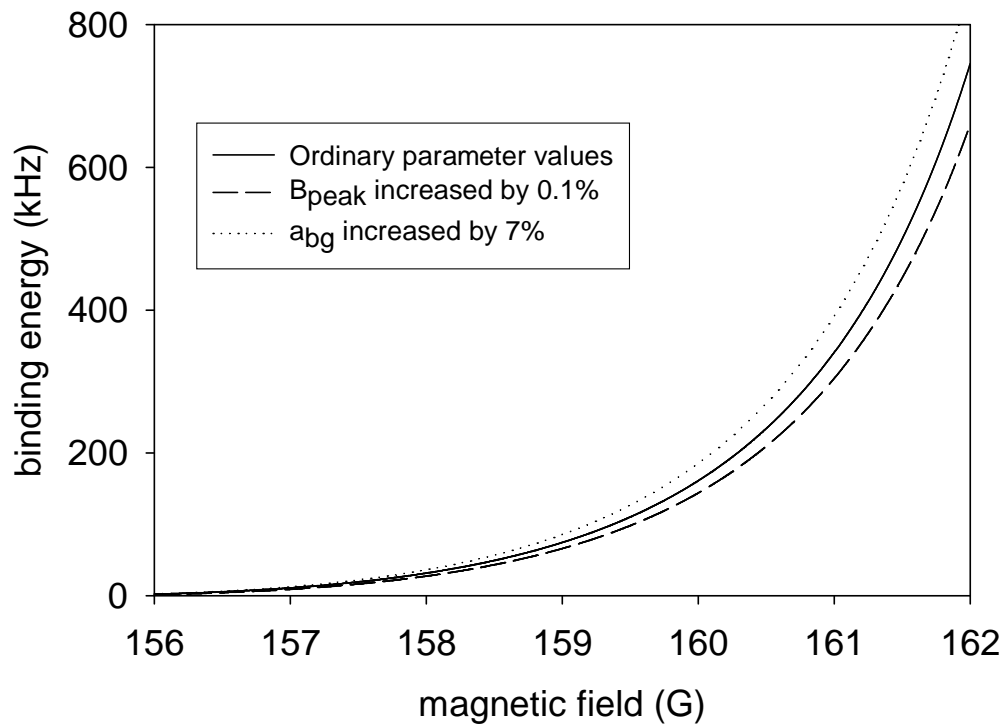


Figure 7.1: Sensitivity of binding energy to Feshbach resonance parameters. The solid line is the binding energy versus magnetic field as calculated from the approximate equation (7.3), with our current best determinations for the Feshbach resonance parameters (section 7.3.3). The dashed line shows the effect of increasing the value of B_{peak} by 0.1% (0.15 G), while the dotted line corresponds to a reduction in $|a_{bg}|$ by 7%. The relative difference in sensitivity to the different parameters can be understood from a simple Taylor expansion of equation (7.3).

providing strong constraints on the exact shape of the interatomic potential.

7.1.3 Advantages of the present method over previous ones

The present method for studying the Feshbach resonance through atom-molecule oscillations offers all of the many inherent advantages of a frequency measurement, including the possibility of high measurement precision, a lack of sensitivity to errors in the absolute atom number calibration, and a simple interpretation of the oscillation frequency in terms of the relative energy difference between the atomic and molecular states. When these advantages are combined with an improved method for magnetic field calibration [3], the present technique for probing the Feshbach resonance is much more precise than previous experiments that examined such Feshbach resonance observables as variable rethermalization rates in a trapped cloud of atoms [75, 13], enhancements of photoassociation rates [74] and inelastic loss rates near the resonance [80], and variations of the mean-field expansion energy of a BEC [12]. In particular, the present atom-molecule coherence experiments have exposed a systematic error in our previous determination of the background scattering length, a_{bg} , as discussed in section 7.3.4. Our new measurement of a_{bg} agrees with the value obtained from an analysis of several other high precision experiments with ultracold rubidium [69].

7.1.4 Improved determination of B_{zero}

To complete the precise characterization of the Feshbach resonance, we also made an improved measurement of B_{zero} , the magnetic field where the scattering length vanishes. This experiment is very similar to our previous work [1, 13, 33], where we determined the $a=0$ field by measuring the critical number (N_{cr}) for collapse of a BEC. For a given magnetic field (scattering length), there is an upper limit to the number of atoms the condensate can contain before becoming unstable. To measure this critical number, we prepare a large ($N_0 \sim 16000$) condensate with fewer than 5% thermal fraction. The

condensate is formed at a B-field where the scattering length is positive ($a \sim 200 a_0$). We next apply an adiabatic magnetic field ramp to change the sign of the scattering length from positive to negative, then we slowly increase the B-field until the condensate collapses, which causes an abrupt drop in the number of atoms. From the measured value of the collapse B-field ($B_{collapse}$) and the known slope of $1/N_{cr}$ versus magnetic field [33] we can extrapolate to the magnetic field where N_{cr} would be infinite, thereby determining the value of B_{zero} . We have improved the measurement precision of B_{zero} by about a factor of 4 by improving our magnetic field calibration and using a larger number of condensate atoms to measure the collapse. We find $B_{zero}=165.750(13)$ G.

7.2 Measuring the B-field dependence of oscillation frequency

7.2.1 Production of BEC and measurement of total number

The procedure used to generate atom-molecule oscillations in ^{85}Rb Bose-Einstein condensates has been described in chapter 6, so we merely outline the method here. After creating condensates with initial number of atoms $N_0 \simeq 16000$ at a magnetic field $B \simeq 162$ G, we apply two short B-field pulses ($\sim 40 \mu\text{s}$ duration) that approach and then recede from the Feshbach resonance at $B_{peak} \simeq 155$ G. The intermediate value of magnetic field between the pulses, B_{evolve} , and the time spacing between pulses, t_{evolve} , are variable quantities. The double pulse sequence is followed by a slow change in the B-field to expand the BEC [2], then the trap is switched off ($B \rightarrow 0$) and destructive absorption imaging is used to count the number of atoms remaining in the condensate.

7.2.2 Atom-molecule oscillations

As in Ref. [4], periodic oscillations in the BEC number were observed as a function of t_{evolve} (see Figure 7.2). We fit the BEC number oscillation to a damped harmonic

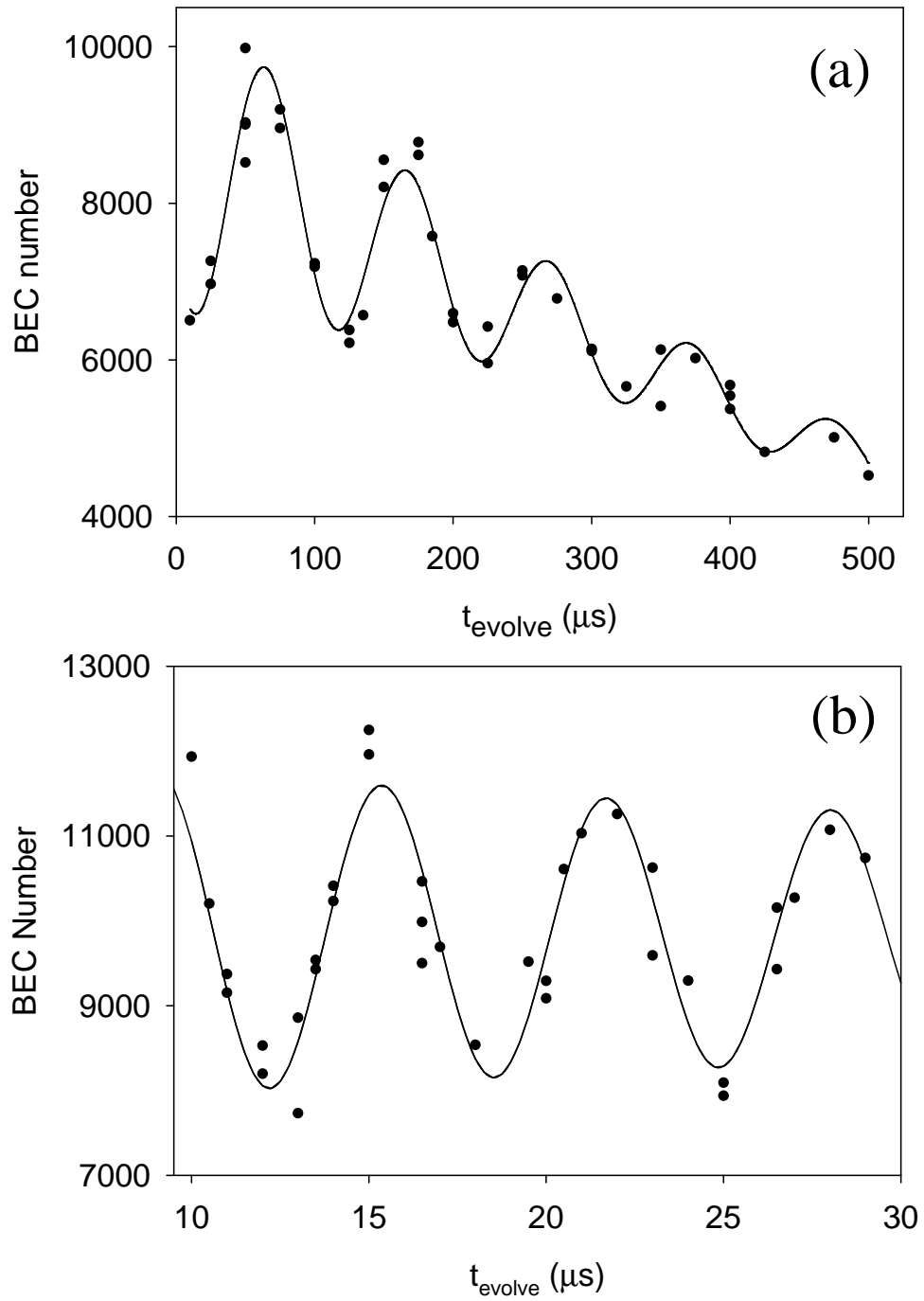


Figure 7.2: BEC number versus pulse spacing t_{evolve} . (a) $B_{\text{evolve}}=156.840(25)$ G. At this magnetic field, which is relatively close to resonance, the oscillation frequency is very low ($\nu_0=9.77(12)$ kHz) so that the damping and atom loss significantly affect the observed time dependence (here $\beta=3640(750)$ s^{-1} and $\alpha=7.9(4)$ atoms/ μs). (b) $B_{\text{evolve}}=159.527(19)$ G. Farther from resonance, the time dependence of the BEC number is dominated by the higher oscillation frequency of $\nu_0=157.8(17)$ kHz. Damping of the oscillations and atom loss are negligible in the relatively short time window used to determine ν_0 .

oscillator function with an additional linear loss term:

$$N(t) = N_{avg} - \alpha t + A \exp(-\beta t) \sin(\omega_e t + \phi), \quad (7.4)$$

where N_{avg} is the average number, A is the oscillation amplitude, α and β are the number loss and damping rates, respectively, and $\omega_e = 2\pi\sqrt{\nu_0^2 - [\beta/(2\pi)]^2}$. The quantity of interest here is ν_0 , the natural oscillator frequency corresponding to the molecular binding energy, $\nu_0 = \epsilon_{bind}/h$.

We measured the oscillation frequency for values of B_{evolve} from 156.1 G to 161.8 G. Over this range, the frequency varies by over 2 orders of magnitude (10-1000 kHz), but the linear loss rate changes very little. The damping rate shows a significant B-field dependence, increasing from $\beta \simeq 2\pi \times 0.8$ kHz near 156 G to $\beta \simeq 2\pi \times 22$ kHz near 162 G. We find no significant density dependence to the damping at $B_{evolve} = 158.60(5)$ G; increasing the total atom density by a factor of 4.3(5) leads to a damping rate increase of only a factor of 1.3(3). Atom loss from the BEC is well described by a linear rate of -2 to -7 atoms/ μ s over the field range of interest. The rate is consistent with previous measurements of number loss due to a single B-field pulse toward the Feshbach resonance, although we have not determined the mechanism for this loss [3].

7.2.3 Limits to precision of frequency measurement

The oscillation frequency measurements have a typical fractional uncertainty of 1%. In principle, the precision of the oscillation frequency determination could be improved indefinitely by increasing the integration time, t_{evolve} . However, there are several effects that prevent us from simply increasing t_{evolve} without limit. First, time variation in the applied magnetic field limits the number of oscillations we can observe. Since we destroy the condensate each time we measure the number of atoms, any variation in B-field from one shot to the next causes the B-field-dependent oscillation frequency to

shift slightly. This frequency shift manifests itself in the BEC number oscillations as a phase shift. If the phase shift between successive measurements is large enough, then the oscillations “wash out” and become impossible to measure. Because the phase shift is proportional to t_{evolve} , our sensitivity to phase noise increases for longer integration time. Evidence for phase noise can be seen in the BEC number oscillations displayed in Figure 7.3.

Another limitation to the precision of the oscillation frequency determination is the finite coherence time for the oscillations. The oscillation amplitude decays with time until the amplitude becomes similar in size to the experimental noise on the number measurement. We typically find that the effects of phase noise dominate over decoherence in limiting the precision of a given frequency measurement, except for the lowest frequency data taken near resonance, where the oscillations damp out on the same time scale as the oscillation period (see section 7.5.1).

In addition to shot-to-shot B-field variations, it is possible to have time variation of the magnetic field during t_{evolve} that is reproducible from shot-to-shot. For example, if the magnetic field from the auxiliary coil is not adjusted to properly compensate for eddy current effects (described in section 3.4.6), the B-field may change as t_{evolve} increases. This variation leads to an oscillation frequency variation or “chirp”. Such a chirp significantly complicates the process of accurately determining the oscillation frequency as a function of magnetic field.

7.2.4 Magnetic field determination

To characterize the Feshbach resonance it is necessary to know B_{evolve} precisely as well as the oscillation frequency. As described in section 3.3, we measure B_{evolve} by transferring atoms to an untrapped spin state by driving $\Delta m = +1$ spin flip transitions with an applied pulse of rf radiation (pulse length = 5 → 25 μs). The spin flip frequency is determined from the rf lineshape for the loss of atoms from the magnetic trap. After

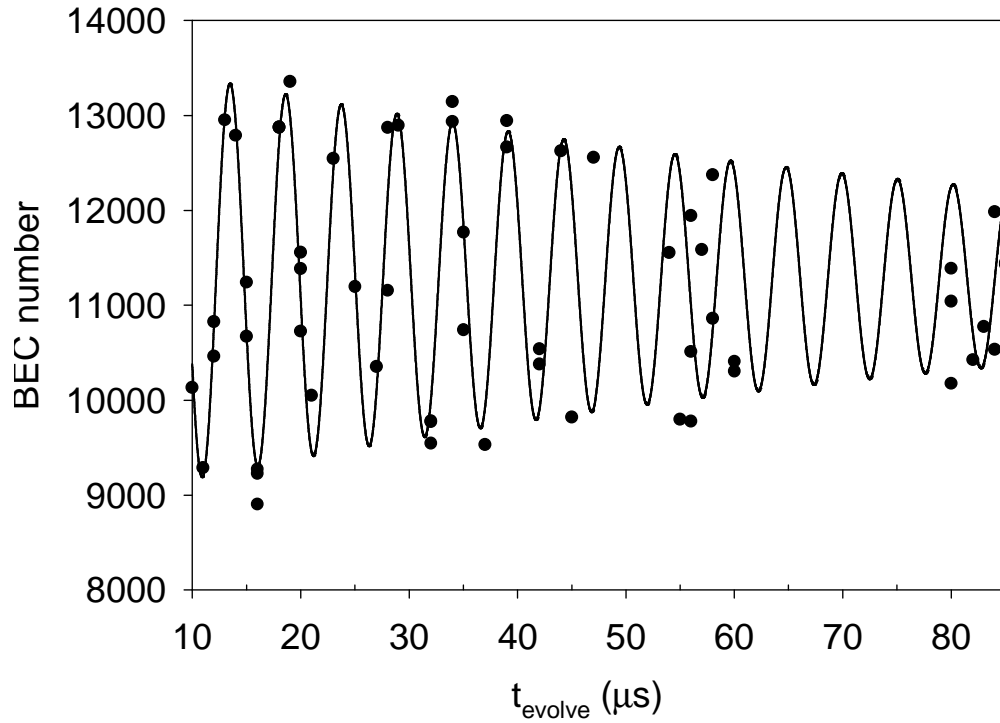


Figure 7.3: Phase noise in BEC number oscillations. Black points are the measured number of BEC atoms versus t_{evolve} while the black line is a fit to the short time data $t_{\text{evolve}} \leq 42 \mu\text{s}$. The scatter in the data near $50 \mu\text{s}$ and $80 \mu\text{s}$ indicates phase noise that is at least π radians in magnitude. From the observed phase noise and the known dependence of frequency on magnetic field, $\Delta\nu_0/\Delta B$, one can estimate the minimum amount of magnetic field noise required. The data near $50 \mu\text{s}$ imply shot-to-shot B-field noise of 0.05 G (peak-peak). Because $\Delta\nu_0/\Delta B$ increases rapidly as the B-field increases above the Feshbach resonance, the higher magnetic field (and higher oscillation frequency) data are more susceptible to phase noise.

measuring the rf transition frequency, we invert the Breit-Rabi equation to obtain the corresponding B-field. To ensure that the magnetic field is sufficiently constant during t_{evolve} , we map out $B(t)$ using rf pulses with lengths short compared to t_{evolve} . Due to interference of the rf radiation with the magnetic field control circuitry, there is a small systematic shift of the field as a function of the rf power used. The uncertainty for each magnetic field determination is the quadrature sum of the uncertainty due to the lineshape measurements (10→15 mG) and the uncertainty in the extrapolation to zero rf power (~20 mG). Typically, the total uncertainty in the average B-field was ~25 mG and was dominated by the rf power shift. Although we were aware of the rf power shift when we gathered the data, at that time we did not realize how the power shift would dominate all other uncertainties in the magnetic field determination. Only after extensive analysis did this become apparent. In the future, it should be possible to reduce the effects of rf interference in the experiment by adding shielding at appropriate places in the auxiliary coil circuit.

7.3 Coupled-channels analysis of data

7.3.1 Coupled-channels theory

To accurately model the nonlinear magnetic field dependence of the binding energy near the Feshbach resonance, a coupled-channels (CC) scattering theory is required. Coupled-channels scattering theory was first applied to ultracold alkali atom collisions by Verhaar and coworkers [81, 8]. This theory offers a full quantum mechanical description of the 2-body scattering process, including the hyperfine and Zeeman Hamiltonians of the separated atoms as well as the short-range molecular interactions and long-range van der Waals interactions. The CC theory can be used to predict the energy and magnetic field dependence of various quantities, such as the phase shift, scattering length, and the energy of molecular bound states. In principle, the accuracy of the CC calcula-

tions is limited only by the incomplete knowledge of the precise shape of the interatomic potentials, which cannot be calculated *ab initio* [82].

The coupled-channels model presented here for ^{85}Rb was developed by Servaas Kokkelmans, who collaborated with us to analyze the magnetic field dependence of the molecular binding energy [83]. Servaas' model is based on the coupled-channels analysis of van Kempen, Kokkelmans, Heinzen, and Verhaar (KKHV) [69], in which several high-precision data for ^{85}Rb and ^{87}Rb were combined to perform an inter-isotope determination of the rubidium interactions with unprecedented accuracy. The predictive power of the KKHV analysis can be seen from Ref. [4], where the initial data on the atom-molecule coherence were already in good agreement with the predicted binding energy of the molecular state. Another example of the accuracy of the KKHV analysis is its agreement with more than 40 Feshbach resonances recently discovered in ^{87}Rb [84].

7.3.2 Fitting the CC model to the data

The measured oscillation frequencies and magnetic fields are listed in Table 7.1 and plotted in Figure 7.4. For the purposes of the coupled-channels fitting, we choose B-field as the independent variable and assume the magnetic field uncertainty, σ_B , is zero. We then increase the frequency error to include the B-field uncertainty according to the formula [85]:

$$\sigma_{\nu, tot} = \sqrt{\sigma_{\nu}^2 + \left(\sigma_B \frac{\partial \nu}{\partial B}\right)^2}, \quad (7.5)$$

where $\frac{\partial \nu}{\partial B}$ is the slope of binding energy versus magnetic field and σ_{ν} and σ_B are the actual measured uncertainties, as given in Table 7.1. For most of the data, the total frequency error ($\sigma_{\nu, tot}$) is dominated by the second term under the square root because of the magnitude of σ_B . This B-field uncertainty comes mainly from a systematic uncertainty related to the rf power shift (section 3.3.4). In fact, the magnetic field error becomes even more significant for the highest oscillation frequency data, where a given

B-field uncertainty corresponds to a much larger frequency uncertainty due to the steep slope of binding energy with B-field (see Figure 7.4). After determining the appropriate uncertainties, we fit the binding energy data and the zero-crossing field B_{zero} to the CC model with a numerical nonlinear regression in Mathematica.

Table 7.1: Measured values of magnetic field and oscillation frequency. The data were combined with a recent measurement of the magnetic field where $a=0$ ($B_{\text{zero}}=165.750(13)$ G). We fit the combined data set with a coupled-channels scattering theory.

B (G)	σ_B (G)	ν (kHz)	σ_ν (kHz)
156.840	0.025	9.77	0.12
158.211	0.025	47.4	1.0
158.655	0.010	73.6	1.1
159.527	0.019	157.8	1.7
160.529	0.021	383.1	3.7
160.887	0.025	509	12
161.771	0.017	1072	11

7.3.3 Extracting Feshbach resonance parameters from best fit

The authors of Ref. [69] used the best known values [13] for the resonant magnetic field B_{peak} and zero crossing B_{zero} . In our analysis, we ignore the relatively imprecise value of B_{peak} from Ref. [13], and instead use the measured dependence of binding energy on magnetic field along with the new B_{zero} measurement given above to determine the interaction parameters. We observe that the fitting procedure is mainly sensitive to only three parameters: the van der Waals dispersion coefficient, C_6 , and the non-integral vibrational quantum numbers at dissociation, v_{DS} and v_{DT} , which determine the position of the last bound state in the singlet and triplet potentials, respectively. Varying the additional parameters C_8 , C_{10} , ϕ_T^E (the first-order energy-dependence of the phase of the oscillating triplet radial wave function), and J , the strength of the exchange interaction, does not improve the fitting because these changes can be absorbed in small shifts of v_{DS} , v_{DT} and C_6 . Therefore, we take the mean values for these four

parameters [86] from the most recent determination in Ref. [84].

The best fit to B_{zero} and the seven highest frequency data points yields a reduced $\chi^2=0.30$ for 5 degrees of freedom. This value of χ^2 is improbably low due to the fact that the uncertainty in the data is dominated by the systematic uncertainty in magnetic field related to the magnitude of the rf power shift. Figure 7.4 shows the resulting theoretical binding energy as a function of the magnetic field together with the experimental values. From the fit, we find substantially improved values for the Feshbach resonance position $B_{\text{peak}}=155.041(18)$ G, width $\Delta=10.71(2)$ G, and background scattering length $a_{\text{bg}}=-443(3)$ a_0 . These results may be compared to previously obtained results $B_{\text{peak}}=154.9(4)$ G and $\Delta=11.0(4)$ G [13], and $a_{\text{bg}}=-450(3)$ a_0 [87]. Our best interaction parameter values are $C_6=4707(2)$ a.u., $v_{DS}=0.00918(17)$, and $v_{DT}=0.94659(29)$. Here the error bars do not include systematic errors due to the uncertainties in other interaction parameters that are not constrained by our data. To compare our values with those of Ref. [69], we determined the sensitivity of our three interaction parameters to systematic shifts in the other parameters, as shown in Table 7.3.3. Using the fractional uncertainties in C_8 , C_{10} , ϕ_T^E , and J from KKHV, we find $C_6=4707(13)$ a.u., $v_{DS}=0.0092(4)$, and $v_{DT}=0.9466(5)$. All of these values agree with those given in KKHV: $C_6=4703(9)$ a.u., $v_{DS}=0.009(1)$, and $v_{DT}=0.9471(2)$. Our value for v_{DS} is more precise than that of Ref.[69], while v_{DT} and C_6 are slightly less precise. However, if future experiments allow improvements to the other interaction parameters, then our results will also become more precise since the systematic errors are comparable to or larger than our statistical errors from the fit.

To understand the strong parameter constraints we obtain with our bound state spectroscopy, it is important to consider the nonlinear dependence of the binding energy on magnetic field. The magnetic field dependence of ϵ_{bind} as it approaches the collision threshold depends sensitively on the exact shape of the long range interatomic potentials, which are mainly characterized by the van der Waals coefficient, C_6 . At

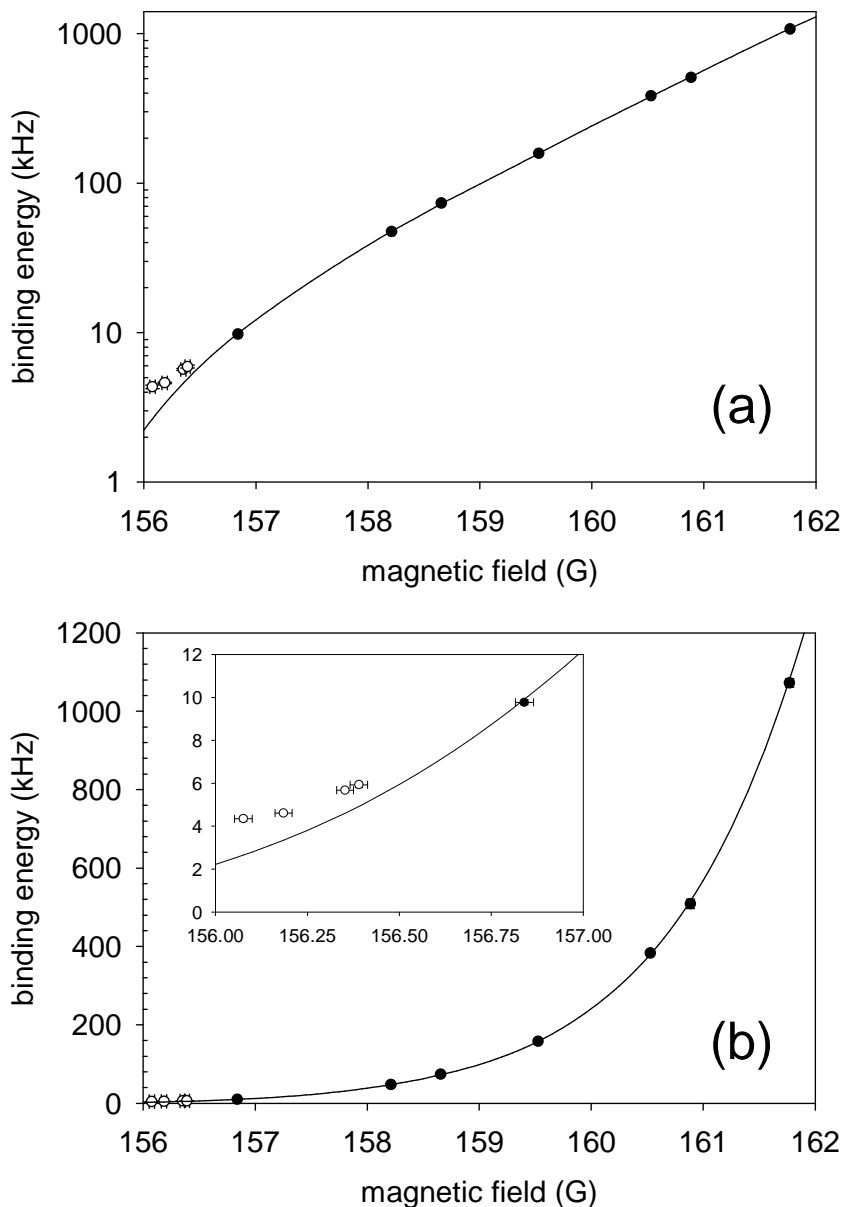


Figure 7.4: Molecular binding energy versus magnetic field, B_{evolve} . (a) The points are measured values of the atom-molecule oscillation frequency, ν_0 , while the solid line represents the molecular binding energy, which we fit to the data by adjusting the parameters of a coupled-channels scattering theory. Only black points were included in the fit; white points were excluded because they experienced a statistically significant mean-field shift. To improve visibility, the points are larger than the error bars. (b) Same as in (a), but with a linear scale for the vertical axis. The inset shows the deviation of the lowest frequency data from the fit to the rest of the data.

Table 7.2: Sensitivity of the determined interaction parameters v_{DS} , v_{DT} and C_6 to fractional uncertainties in C_8 , C_{10} , ϕ_T^E and J . For instance, the systematic error in C_6 due to a 10% uncertainty in C_8 is $123 \times 0.10 = 12.3$ a.u.

	$\Delta C_8/C_8$	$\Delta C_{10}/C_{10}$	$\Delta \phi_T^E/\phi_T^E$	$\Delta J/J$
Δv_{DS}	-1.53×10^{-4}	-6.80×10^{-5}	-2.59×10^{-3}	1.72×10^{-3}
Δv_{DT}	-4.14×10^{-4}	-1.39×10^{-4}	2.31×10^{-3}	1.71×10^{-3}
ΔC_6	123	33.4	-47.8	19.3

magnetic fields far from resonance, the bound state wave function is confined to short internuclear distance and the binding energy varies linearly with magnetic field. The linear dependence on B-field gives relatively little information about C_6 . As the B-field approaches resonance, the detuning decreases until the bound state lies just below threshold. Now the bound state wave function penetrates much deeper into the classically forbidden region, which causes ϵ_{bind} to curve toward threshold as a function of magnetic field. Because the energetically forbidden region stretches out as C_6/r^6 , the observed curvature depends sensitively on the C_6 coefficient. One can show [17] that an analytical Feshbach model that includes the correct potential range and background scattering processes [56] can reproduce the binding energy curve over the full range of magnetic field.

7.3.4 Revised stability prediction for condensates with $a < 0$

As a result of the improved determination of the ^{85}Rb Feshbach resonance parameters, we find that our new value for the off-resonant or background scattering length, $a_{bg} = -442.9(23) a_0$, is inconsistent with the value given in Ref. [13], where $a_{bg} = -380(21) a_0$. The most plausible explanation we can find for disagreement is that the theoretical expression used to relate measured rethermalization rate to cross section [1] is insufficient for the requisite level of accuracy. However, the new value for a_{bg} allows us to revise our previous estimate for the stability condition of a BEC with negative scattering length [33]. We use equation (7.1) to obtain the linear slope of scattering

length versus B-field near $B=B_{zero}$. We then find the stability coefficient for BEC collapse, $k_{collapse}$, by combining the value of $\Delta a/\Delta B=-39.86(22)$ a_0/G with the measured slope of $1/N_{crit}$ versus magnetic field [33] of $0.00128(3)$ $(\text{atoms G})^{-1}$. Thus, we obtain the revised value $k_{collapse}=0.547(58)$, where the error is dominated by a 10% systematic uncertainty in the determination of N_{crit} . The present determination agrees with the theoretical value of 0.55 [88].

7.4 Search for collective effects: mean field shifts

7.4.1 Inadequacy of 2-body scattering theory

The coupled-channels theory used in this work applies to 2-body scattering; therefore, this theory cannot account for many-body effects in the atom-molecule BEC system, such as a mean-field shift to the observed oscillation frequency [9, 68]. Any such mean-field shift must be fractionally largest near the Feshbach resonance, where the coupled-channels theory predicts that the binding energy approaches zero while the atom-atom scattering length increases to infinity. We searched for a mean-field shift to the oscillation frequency when B_{evolve} was decreased to ~ 156 G. As shown in Figure 7.4, the lowest magnetic field data display a clear frequency shift with respect to the coupled-channels theory prediction. As B_{evolve} approaches resonance, the observed shift increases to 1.7 kHz, which significantly exceeds a simple estimate for the average atom-atom mean-field shift in the BEC: $4\pi\hbar^2\langle n \rangle a/m \simeq 0.5$ kHz at $B_{evolve}=156.1$ G. We expect the mean-field shift to depend on the density of atoms (and molecules), but we have not yet studied the density dependence. In practice, the initial BEC density can be changed by adiabatically varying the initial scattering length before the rapid magnetic field pulses as discussed in section 5.3.3.

7.4.2 Statistical method for determining mean-field shifts

Since the lowest frequency data show evidence for a mean-field shift, we exclude these points from the (2-body) theory fit. We determine the cutoff magnetic field for the excluded region by the following procedure. First, we fit the data set that includes all frequency measurements satisfying $\nu_0 \geq 73$ kHz. For these data, the expected fractional effect of any mean-field shift is negligible; for example, the average mean-field interaction energy in the atom BEC is ≤ 0.1 kHz, and we expect atom-molecule interactions to be similar in magnitude. After fitting this minimal data set, we add the next lower frequency/B-field measurement to the data set and repeat the theory fit. Finally, we compare the two fits according to their minimum χ^2 values. As long as the increase in χ^2 that results from addition of a new data point is reasonable (on the order of unity), we conclude that there is no significant mean-field shift associated with the frequency measurement.

Table 7.3: Total χ^2 and B_{peak} as a function of the number of included data points in the coupled-channels fit. The abrupt jump in χ^2 and B_{peak} as the data set increases from 7 to 8 points indicates the presence of a mean-field frequency shift in the 8th point. The mean-field shift magnitude increases as the added points approach closer to the Feshbach resonance; since the shift is non-statistical, χ^2 increases very rapidly as more points are added to the set.

Included pts.	Total χ^2	B_{peak} from fit
5	0.42	154.971
6	0.77	154.994
7	1.3	155.042
8	10.0	154.965
9	15.4	154.922
10	24.4	154.885
11	41.7	154.847

In Table 7.3 we give the variation of total χ^2 and B_{peak} as a function of the number of points included in the fit. Both χ^2 and B_{peak} shift abruptly when the number of points increases from 7 to 8 (corresponding to a decrease in B_{evolve} from 156.840 G

to 156.390 G). The observed behavior seems sensible since we expect mean-field shifts to increase rapidly as one moves toward resonance (see Figure 7.4). Our χ^2 exclusion criterion allows us to fit the data in a manner that avoids systematic errors in the Feshbach resonance parameters. By extrapolating the coupled-channels binding energy prediction to lower magnetic fields, we determine the magnitude of the mean-field shifts, which are listed in Table 7.4.

Table 7.4: Measured values of magnetic field and corresponding mean-field shifts to the molecular binding energy. The mean-field shifts were determined by subtracting the extrapolated coupled-channels binding energies from the lowest oscillation frequency data. The shift error, σ_{mf} , is simply the error from the frequency measurement.

B (G)	σ_B (G)	$\Delta\nu_{mf}$ (kHz)	σ_{mf} (kHz)
156.076	0.024	1.69	0.12
156.185	0.023	1.26	0.06
156.352	0.023	1.07	0.08
156.390	0.024	1.00	0.13
156.840	0.025	-0.15	0.12

7.5 Low frequency oscillations: a simple model

7.5.1 Damping of oscillations: experiment and theory

The low frequency oscillations that show evidence for a mean-field shift are quite strongly damped, so only one or two wiggles are observed before the signal-to-noise ratio approaches unity. In addition, the number loss rate, $\alpha \simeq 7$ atoms/ μ s, causes a significant decrease in the average number of BEC atoms during t_{evolve} . The combination of these effects leads to a rather complicated time dependence of the measured BEC number, as shown in Figure 7.5.

We use a simple model to explain part of the observed damping as due to inhomogeneous dephasing from a density dependent mean-field shift. This idea was suggested to us by Murray Holland and Servaas Kokkelmans [9]. Assuming that the atom-molecule

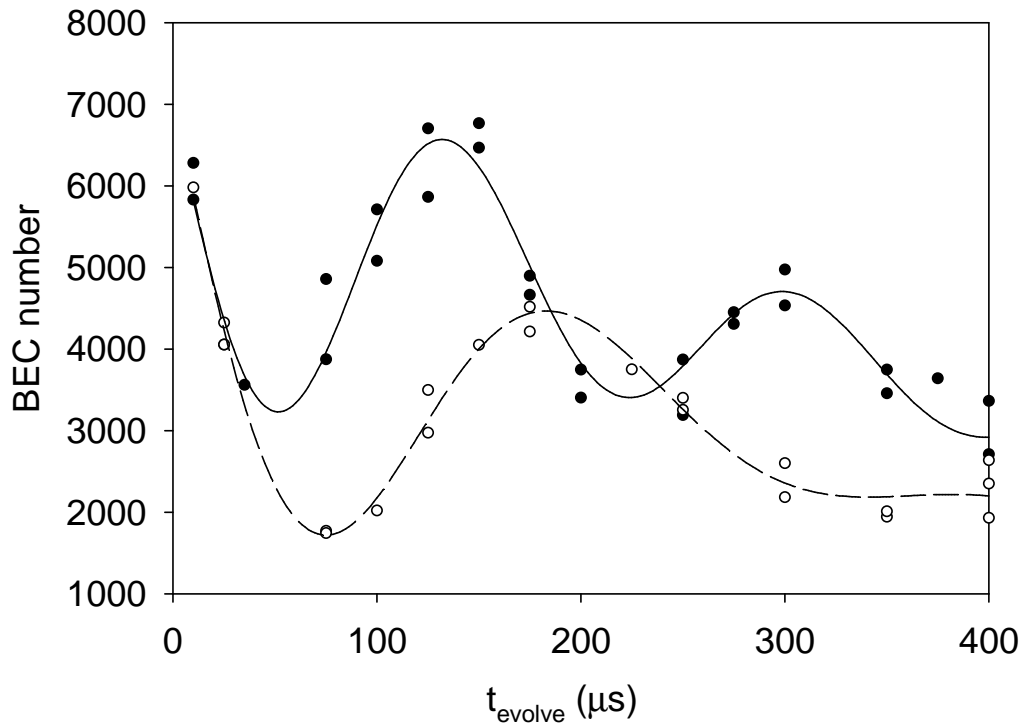


Figure 7.5: Low frequency BEC number oscillations. Black points correspond to $B_{\text{evolve}}=156.390(24)$ G; white points were at a lower magnetic field of $B_{\text{evolve}}=156.076(24)$ G. The solid line is a fit to the black points using equation (7.4) with $\nu_0=5.93(13)$ kHz, $\beta=4500(1200)$ s $^{-1}$ and $\alpha=6.1(8)$ atoms/ μs . The dashed line fit to the white points gives parameter values of $\nu_0=4.34(12)$ kHz, $\beta=7600(1000)$ s $^{-1}$, and $\alpha=6.4(5)$ atoms/ μs .

oscillation frequency depends on the local density in the sample, we have

$$\nu(\vec{r}) = \nu_{bare} + An(\vec{r}), \quad (7.6)$$

where ν_{bare} is the “bare” oscillation frequency at zero density (i.e., the molecular binding energy), A is the (positive) frequency shift per density and is determined empirically, and $n(\vec{r})$ is the local density in the BEC cloud. For simplicity, we assume that the density distribution of the condensate has an isotropic parabolic form:

$$n(\vec{r}) = \begin{cases} n(0)[1 - r^2/R^2] & r \leq R \\ 0 & r > R \end{cases} \quad (7.7)$$

where $n(0) = \frac{15N}{8\pi R^3}$ is the peak density, N is the total number of atoms, and R is the radius of the parabolic condensate. Although we neglect the anisotropy of the BEC, this is a fairly reasonable approximation since the aspect ratio is at most 2.5 in the Thomas-Fermi limit (we approximate a football-shaped object by a sphere). The Thomas-Fermi approximation of a parabolic density distribution is well satisfied by the condensates since we typically prepare them at the evaporation magnetic field of 162.3 G, corresponding to $a \sim 200 a_0$. For this scattering length, the ratio of mean field interaction energy to kinetic energy in the BEC is $Na/a_{ho}=55$, which is far into the Thomas-Fermi limit.

Using the above density distribution, we next obtain the probability distribution of the atoms in oscillation frequency space. We simply find the probability of being in a given spherical shell of constant density (constant frequency). The probability per unit frequency is

$$P(\nu) = \frac{2\pi R^3}{NA} \frac{(\nu - \nu_{bare})}{\Delta\nu_{max}} \sqrt{1 - \frac{(\nu - \nu_{bare})}{\Delta\nu_{max}}}, \quad (7.8)$$

where $\Delta\nu_{max} = An(0)$ is the maximum frequency shift corresponding to the peak density in the sample and $P(\nu)$ is normalized so that $\int_0^{\nu_{bare} + \Delta\nu_{max}} P(\nu) d\nu = 1$.

After obtaining the probability distribution in equation (7.8), we numerically calculate the Fourier transform of $P(\nu)$ and study the oscillation amplitude versus time.

One can then look for the effects of density-dependent dephasing in the oscillations.

7.5.2 Comparison of dephasing model to data

In Figure 7.6, we plot the theoretical oscillation amplitude as a function of time for two choices of the quantities ν_{bare} and $\Delta\nu_{max}$. We chose these values based on empirical estimates for the mean-field shift — we estimated the average shift by extrapolating the coupled-channels prediction for ϵ_{bind} and then calculating the difference between this prediction and the measured oscillation frequency.

The dephasing model predicts damped oscillations that are qualitatively similar to the experimental measurements, as can be seen by comparing Figures 7.5 and 7.6. To make a more quantitative test of the dephasing model predictions, we show the mean-field shift and damping rate versus magnetic field in Figure 7.7. Here the observed oscillation frequency shifts and damping rates can be directly compared to the predictions of the dephasing model. Figure 7.7 demonstrates that the damping rates predicted from the dephasing model are significantly smaller than those observed in the experimental data. There appears to be an additional B-field-independent damping mechanism in the experiment. The most obvious additional source of damping is the observed loss of BEC atoms during the evolution time between magnetic field pulses. This loss has no apparent B-field dependence over the range of magnetic fields in Figure 7.7. Although the mechanism for the loss is unknown, the process must be distinct from that of the inhomogeneous dephasing discussed here and should lead to a loss of coherence in the oscillations.

7.5.3 Additional damping from atom loss

To predict the expected damping rate due to the measured atom loss rate, we assume that the only the atomic state in the atom-molecule superposition experiences decay of population. One can show [89, 90] that if the number of atoms decreases at

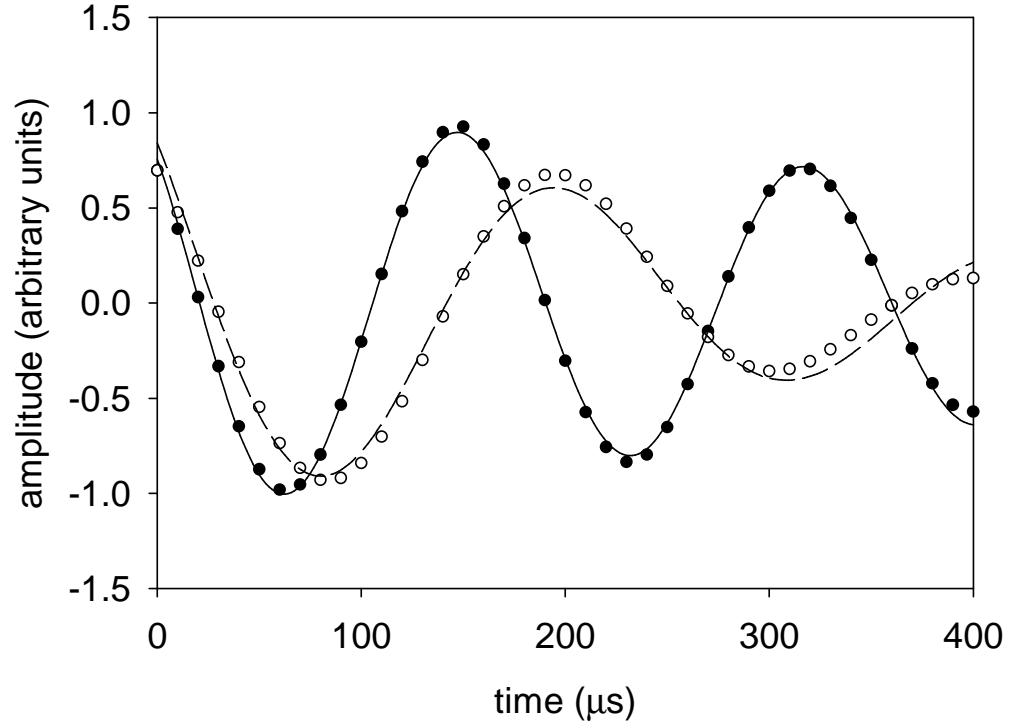


Figure 7.6: Theoretical model for density-dependent dephasing. Points are the calculated Fourier transform of the frequency probability distribution in equation (7.8) versus time. A phase shift of 0.8 rad was added to the Fourier transform to better approximate the initial phase in the experiment (see Figure 7.5). The black points correspond to a bare oscillation frequency of $\nu_{bare}=4.9$ kHz with an average mean-field shift of $\Delta\nu=0.99$ kHz. The white points had $\nu_{bare}=2.7$ kHz and $\Delta\nu=1.7$ kHz. The solid and dashed lines are fits to the two different model data sets. From these fits, we extract values for the oscillation frequency of an equivalent damped oscillator, ν_0 (see equation(7.4)), and its damping rate, β . The fits yield $\nu_0=5.90(1)$ kHz and $\beta=2250(120)$ s $^{-1}$ (solid line) and $\nu_0=4.42(3)$ kHz and $\beta=3560(220)$ s $^{-1}$ (dashed line). The fits allow us to compare the dephasing model directly to the data.

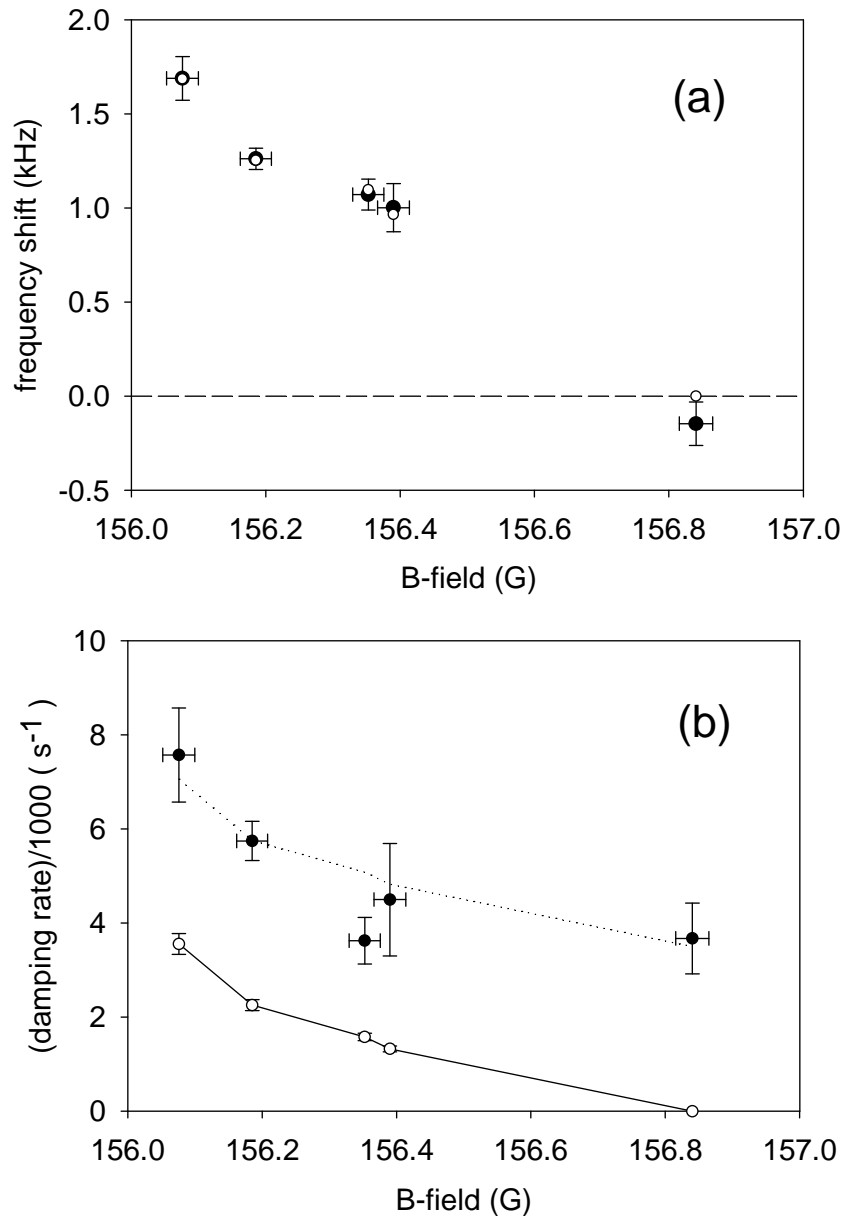


Figure 7.7: Comparison of data and theory for oscillation damping rates versus B-field. **(a)** Mean-field shift of the oscillation frequency as a function of magnetic field. Black points with error bars are empirically determined values of the mean-field shift, as discussed in the text. White points are the values of the mean-field shift used in the dephasing model. **(b)** Damping rates versus B-field. Black points with error bars are damping rates from fitting the BEC number oscillation data, as in Figure 7.5. White points connected by straight lines are the predicted damping rates due to inhomogeneous dephasing from the mean-field shifts in part **(a)**. The dotted line shows the effect of adding a constant rate of 3500 s^{-1} to the dephasing model prediction.

an exponential rate, $N_a = N_0 \exp(-\gamma t)$, the amplitude for population oscillations will decay according to $\exp(-\gamma t/2)$. In the magnetic field range of interest (from 156-157 G), we observed a roughly linear loss rate from the atom BEC of $-\alpha = -7.2$ atoms/ μs . To convert this linear loss rate into an effective exponential decay rate, we determine the time interval required to decrease the total number of BEC atoms by a factor of $1/e$. The initial average number of BEC atoms at our shortest evolution times ($t_{\text{evolve}} \simeq 0$) was 6000, so the time to reach $6000/e = 2210$ with a linear loss rate of -7.2 atoms/ μs is $527 \mu\text{s}$. This $1/e$ time corresponds to an effective number decay rate of $\gamma = 1900 \text{ s}^{-1}$, so we expect the atom-molecule oscillations to decay at the rate $\gamma/2 = 800 \text{ s}^{-1}$.

As can be seen from Figure 7.7, the additional damping rate due to atom number loss is too small to explain the discrepancy between the data and the simple dephasing theory. In fact, to explain the observations, there must be an additional damping rate of $\sim 3500 \text{ s}^{-1}$, which is more than 4 times larger than the expected damping from decay of the BEC number. There may be other sources for decoherence in the system, including a possible loss from the molecular state during t_{evolve} . Whatever the source of the additional damping, our data suggest that this damping is not strongly sensitive to magnetic field. We also have evidence that the additional damping rate is insensitive to density — at $B_{\text{evolve}} = 158.60(5) \text{ G}$, where the mean-field shift is negligible, we find that increasing the BEC density by a factor of 2.5(3) leads to a damping rate increase of only a factor of 1.24(25). Future investigation of the mean-field shifts and damping rates should improve our understanding of the physics of atom-molecule decoherence near the Feshbach resonance.

7.5.4 Magnitude of mean-field shifts

The magnitude of the mean-field shift shown in Figure 7.7 increases as the magnetic field approaches the Feshbach resonance. Over the 1 G range shown in this figure, the shift increases from 0 to 1.7 kHz. The shift for the lowest magnetic field data is

significantly larger than one would expect from a simple estimate of the average mean-field energy in the BEC, based on the GP equation: $4\pi\hbar^2\langle n\rangle a_{\text{evolve}}/m \simeq 0.5$ kHz at $B_{\text{evolve}}=156.1$ G. The observed shift also exceeds a recent calculation for the equilibrium mean-field shift using an effective quantum field theory [68] (<0.1 kHz). One intriguing possibility for the discrepancy is that there is a positive mean-field shift due to atom-molecule (or molecule-molecule) interactions. We believe that the current data are interesting and suggestive, but we have really only touched the tip of the iceberg in this area.

Since a mean-field shift must depend on the density of atoms and molecules, it would be desirable to study the density dependence. Ideally, one would like to change the density of atoms and molecules independently to identify the source of the shift(s). At the present time, we have not measured any density dependence to the mean-field shifts.

7.5.5 Limitations of current method and possible future experiments

As discussed above, the observed time dependence of the BEC number arises from the interplay between the bare atom-molecule oscillation frequency and a density-dependent frequency shift. The data suggest the presence of highly interesting many-body physics, but the information we can glean from the oscillation data is limited. For example, as we decrease the magnetic field to approach closer to the Feshbach resonance, we observe that the oscillations rapidly damp out due to increased dephasing. Eventually the damping rate becomes comparable to the oscillation frequency and it becomes impossible to reliably extract the underlying frequency because the system is critically damped. One way to avoid this limitation would be to measure the atom-molecule oscillations as a function of position in the condensate. If we could “bin” the cloud into different spatial regions, then we could avoid the effect of inhomogeneous dephasing [89]. However, our present method of measuring the BEC number involves a large

time-of-flight expansion before imaging, which effectively blurs any spatial information about the pre-expansion condensate (see section 3.5.3).

Another practical limitation of our experiment comes from the finite amount of charge stored in the capacitor bank used to control the magnetic field (see section 3.4.3). The finite amount of charge prevents us from holding the magnetic field constant for more than ~ 1 ms, so we cannot observe an atom-molecule oscillation with a period longer than this limit.

However, we are investigating novel techniques to determine mean-field shifts to the atom-molecule system near the Feshbach resonance. For example, it may be possible to use rf pulse spectroscopy, as discussed in section 3.3.5, to measure the mean-field energy. Such a method allows one to probe the energy of the system on shorter timescales and has proven useful in studies of ^{40}K Feshbach resonances [91].